ELSEVIER

International Journal of Mass Spectrometry 185/186/187 (1999) 533–543

International Journal of Mass Spectrometry

Vacuum ultraviolet single-photon and ultraviolet nonresonant two-photon pulsed field ionization photoelectron study of CH_3SCH_3

Y.-S. Cheung[a,b], C.Y. Ng[a,b,*]

[a]*Ames Laboratory, United States Department of Energy, Iowa State University, Ames, Iowa 50011, USA*
[b]*Department of Chemistry, Iowa State University, Ames, Iowa 50011, USA*

Received 15 June 1998; accepted 28 July 1998

Abstract

The vacuum ultraviolet (VUV) single-photon and ultraviolet nonresonant two-photon (N2P) pulsed field ionization photoelectron (PFI-PE) spectra for CH_3SCH_3 have been obtained in the energy range of 69 500–72 500 cm^{-1}. Vibrational structures observed in the VUV-PFI-PE and N2P-PFI-PE spectra are similar. Guided by the ab initio theoretical harmonic frequencies, we have assigned the vibrational bands resolved in these spectra. Using a semiempirical simulation scheme, together with ab initio theoretical rotational constants for CH_3SCH_3 and $CH_3SCH_3^+$, we have also obtained a good fit to the contours of rotational branches resolved in the origin band of the VUV-PFI-PE spectrum. Taking into account the uncertainty of the simulation model used, we obtain a value of 70 097.3 ± 2.0 cm^{-1} (8.69096 ± 0.00016 eV) for the adiabatic ionization energy of CH_3SCH_3. (Int J Mass Spectrom 185/186/187 (1999) 533–543) © 1999 Elsevier Science B.V.

Keywords: Photoionization; Photoelectron; Ionization energy

1. Introduction

Accurate ionization energies (IE's) for molecular species, which are used for prediction of chemical reactivity, are of fundamental importance to chemists [1,2]. The IE of a gaseous molecule can be determined routinely in a photoionization [2] or a photoelectron [3,4] experiment. Ionization energy determinations made in conventional photoionization and photoelectron studies have uncertainties in the range of 3–100 meV (25–250 cm^{-1}). The accuracy of adiabatic IE values measured for polyatomic molecules is especially poor because of the difficulty in assessing the hot band and kinetic shift effects [2]. The fact that the geometries for a neutral polyatomic molecule and its cation are usually different often makes photoionization yields very low near the ionization threshold. The combination of these effects may prevent the observation of the ionization step in the photoionization efficiency (PIE) spectrum of a polyatomic molecule, and thus results in a large uncertainty in the experimental IE value [5]. Recent advances in ab initio quantum computation procedures [6,7], such as the GAUSSIAN-2 (G2) type theories [6] and density functional [8] theoretical methods, have been able to provide IE predictions for small polyatomic molecules and radicals of main group elements to an

* Corresponding author. E-mail: cyng@ameslab.gov

Dedicated to Professor Michael T. Bowers on the occasion of his 60th birthday.

PII S1387-3806(98)14124-6

accuracy of <0.15 eV, approaching that achievable in conventional photoionization and photoelectron experiments. This theoretical achievement has set a challenge for experimental IE measurements to be made with higher accuracy.

In the past decade, the most exciting development in the field of photoionization and photoelectron spectroscopy has been the availability of high resolution, tunable ultraviolet (UV) and vacuum ultraviolet (VUV) laser sources [9–11]. For probing electronic structures of cations, photoelectron spectroscopic measurements are preferred over PIE studies. The laser pulsed field ionization photoelectron (PFI-PE) scheme is the current state-of-the-art photoelectron spectroscopic technique, and is capable of providing photoelectron energy resolution close to the optical resolution [12–14]. For specific molecular species with IE values below 12 eV, the nonresonant two-photon (N2P) PFI-PE scheme involving the use of a UV laser is an attractive method for high resolution photoelectron measurements [15,16]. Without doubt, the single-photon PFI-PE technique is the most versatile high-resolution photoelectron spectroscopic method. In the current technical level, VUV laser radiation with usable intensities can be generated at energies up to $\approx$17.7 eV by nonlinear optical mixing using commercial dye lasers [9]. Most recently, a synchrotron based VUV-PFI-PE technique has also been demonstrated using monochromatized third-generation undulator synchrotron radiation at the photon energy range of 8–27 eV [17,18]. The PFI-PE resolutions achieved in synchrotron, UV laser, and VUV laser based measurements are similar. For specific diatomics, triatomics, and simple hydrides, N2P-PFI-PE and VUV-PFI-PE measurements have provided IE values with uncertainties less than a few cm^{-1} [12,19]. This accuracy represents a 10–100-fold improvement over those achieved in conventional photoionization and photoelectron measurements. In principle, the analysis of a truly rotational resolved photoelectron spectrum of a molecule is expected to yield the definitive IE value.

Despite this impressive experimental progress in high-resolution photoelectron spectroscopy, the photoelectron energy resolutions [>0.2 cm^{-1}, full width at half maximum (FWHM)] obtainable in laser or synchrotron based PFI-PE measurements are still not sufficient to resolve rotational transitions in photoelectron spectra of polyatomic molecules. Thus, PFI-PE studies of polyatomic species reported today mostly provide vibrational information for the corresponding cations [12]. In recent VUV-PFI-PE and N2P-PFI-PE studies of CH_3SH and CH_3CH_2SH, we find that the FWHM for individual vibrational bands are in the range of 15–25 cm^{-1} for supersonically cooled CH_3SH and CH_3CH_2SH samples at rotational temperatures of 20–30 K [20,21]. These experiments also show that the resolution achieved in the VUV-PFI-PE measurement is better than that in the N2P-PFI-PE study performed under similar experimental conditions [21]. Fine structures arising from contours of rotational branches are resolved in the origin bands of the VUV-PFI-PE spectra for CH_3SH and CH_3CH_2SH. The simulation of these fine structures has provided accurate IE values for CH_3SH and CH_3CH_2SH with uncertainties of ± 2.9 cm^{-1} [21].

Here, we present the results of an N2P-PFI-PE and VUV-PFI-PE study of CH_3SCH_3. As in previous studies [20,21], ab initio predictions for vibrational and rotational constants of CH_3SCH_3 and $CH_3SCH_3^+$ are used to assist the assignment and simulation of the PFI-PE spectra. Theoretical predictions obtained using standard ab initio program packages [22] for vibrational and rotational constants for small polyatomic species are known to have an accuracy of 10–20%. This experiment, together with previous studies [20,21,23], suggests that with an achievable instrumental resolution of $\approx$0.5–1.0 cm^{-1}, it is advantageous to perform PFI-PE measurements of polyatomic molecules at higher rotational temperatures. The rotational contours resolved in a rotationally hot spectrum contain more information about the rotational structures of the neutral and cationic species as compared to that observed in a rotationally cooled spectrum.

2. Experiment and ab initio calculations

The experimental apparatus and procedures used are similar to those described previously [20,21,23–

25]. The apparatus consists of a tunable UV or VUV laser source, a pulsed molecular beam source, an ion time-of-flight (TOF) mass spectrometer, and an electron detector for PFI-PE detection.

2.1. VUV-PFI-PE and VUV-PIE measurements

The VUV laser system has been described previously in detail [21,25]. Briefly, it is comprised of one excimer laser (Lambda Physik EMG201), two dye lasers (Lambda Physik FL3002), and a Xe gas cell for nonlinear optical mixing. The XeCl excimer laser output (308 nm, 200–250 mJ) was split to pump the two dye lasers. For the present study on CH_3SCH_3, the photon energy range of interest is 69 900–71 500 cm^{-1}. The UV frequency ω_1 was generated using coumarin-450 dye in one of the dye lasers followed by frequency doubling with a BBOI crystal. Here, UV frequency was fixed at $2\omega_1 = 89860.6$ cm^{-1}, corresponding to the two-photon resonance of the Xe 5p → 6p transition. The other dye laser is tuned in the visible frequency (ω_2) range of 18 200–20 800 cm^{-1} that was generated using coumarin-500 dye. The visible laser beam is merged with the UV laser beam by a dichromic mirror. Both beams were then focused into the Xe gas cell (pressure ≈ 21 Torr) by a focusing lens (focal length = 15 cm). The VUV frequencies (ω_{VUV}) were produced by the four-wave difference frequency ($\omega_{VUV} = 2\omega_1 - \omega_2$) mixing in the Xe gas cell. The gas cell has a quartz entrance window and a MgF_2 exit window that serves to isolate the gas cell from the photoexcitation/photoionization (PEX/PI) chamber. With a transmission cutoff wavelength of ≈115 nm, the MgF_2 window allows the VUV difference frequencies to transmit while absorbing the VUV sum frequencies.

A photoelectric detector made out of Cu was used to measure the VUV laser photon intensities. In addition to monitoring the VUV light intensities, the photoelectric detector also served as a light trap for ω_1, ω_2, and ω_{VUV}. However, by blocking the visible laser beam, we found that ≈90% of the photoelectric current is contributed by the UV laser (ω_2) beam. Fortunately, this background is nearly constant because the UV frequency is fixed. We found that the intensity of the VUV difference frequency is also nearly constant over the VUV range of interest here. The VUV-PFI-PE intensities presented here were not normalized by the corresponding VUV light intensities.

To calibrate the laser frequencies, a small fraction of the dye laser (ω_2) output was directed into a uranium hollow cathode lamp with Ne as the buffer gas. The Ne absorption spectrum recorded simultaneously during the experiment provided accurate energy calibration of the PFI-PE spectra. The bandwidth of the dye laser is 0.2 cm^{-1} for the fundamental and ≈0.4 cm^{-1} for the second harmonic output. For a two-photon excitation, the resolution is ≈0.8 cm^{-1}. Thus, the resolution for the VUV laser radiation is estimated to be ≤1 cm^{-1}. The accuracy of photon frequency calibration is expected to be ±0.2 cm^{-1}.

The photoelectron–photoion apparatus [20,21,23,24] used in this study consists of a pulsed molecular beam production system, an ion TOF mass spectrometer, and an electron detector for PFI-PE detection. The molecular beam source chamber was pumped by a freon-trapped, 6 in. diffusion pump (pumping speed ≈2000 L/s), while the photoionization chamber and the ion TOF tube were evacuated by turbomolecular pumps with pumping speeds of 250 L/s and 50 L/s, respectively. During the experiment, the beam source chamber and the photoionization chamber were maintained at pressures of ≈5×10^{-5} and ≈5×10^{-7} Torr, respectively.

Ion detection using the ion TOF mass spectrometer has been described previously [23,24]. In this study, a constant electric field at 42 and 167 V/cm was used to extract ions formed in the PEX/PI region. The PFI-PE detection scheme relies on delayed PFI of long-lived high-*n* Rydberg states populated by laser excitation at a few wave numbers below the ionization threshold [12–14]. In the present experiment, the firing of the excitation laser was delayed by 580 μs with respect to the triggering pulse for opening the pulsed valve. After a typical delay of 2.5 μs with respect to firing of the VUV laser, a forward biased pulsed electric field of 0.24 V/cm and 1 μs duration was used to field ionize the high-*n* Rydberg species as well as to extract the electrons to the micro-channel plate detector.

Using this PFI-PE detection scheme, we expect to achieve a resolution of 1.0–1.5 cm^{-1} (FWHM).

Two digital delay units (Stanford Research DG535) control the operating sequence of the pulsed valve, dye laser, and pulsed electric field. The signals from the electron detector (or ion detector) and the photoelectric VUV detector were fed into two identical boxcar integrators (Stanford Research SR250) that were interfaced to an IBM computer.

In this experiment, the CH_3SCH_3 molecular beam was produced by seeding the CH_3SCH_3 vapor (≈430 Torr) at ≈20°C in 640 Torr of Ar and then expanding the mixture through the nozzle (diameter = 50 μm) of a pulsed valve. The CH_3SCH_3 sample (>99% purity) was obtained from Aldrich and used without further purification. The molecular beam is skimmed by a conical skimmer (1 mm diameter, 3.8 cm from the nozzle) before intersecting with the VUV laser beam at 90° and 8.3 cm downstream from the skimmer.

2.2. N2P-PFI-PE measurements

The experimental setup and conditions in the N2P-PFI-PE study [20,23,24] were the same as those in the VUV-PFI-PE study as described above except that only one UV dye laser was used for excitation. Rhodamine-560 dye was used to produce visible light in the range of 17 400–18 100 cm^{-1} (552–575 nm). The second harmonic radiation in the UV range of 34 800–36 200 cm^{-1} was generated using a BBOI crystal. The UV laser radiation thus formed was focused into the PEX/PI region with a 200 mm fused-silica focusing lens (focal length = 200 mm). The typical UV laser pulse energy used was ≈1.2 mJ.

2.3. Ab initio calculations

Ab initio calculations were performed on CH_3SCH_3 and $CH_3SCH_3^+$ with the GAUSSIAN 94 program for Windows installed on a Pentium 166 PC [22]. The G2 energies for CH_3SCH_3 and $CH_3SCH_3^+$ were calculated to obtain the adiabatic IE for CH_3SCH_3. The detail of the G2 procedure has been described previously [6]. The harmonic vibrational frequencies of $CH_3SCH_3^+$ at the MP2/6-31G(d) level were scaled [26] by 0.92 and are employed for the assignment of the vibrational structures obtained in the PFI-PE spectra.

The theoretical geometries of CH_3SCH_3 and $CH_3SCH_3^+$ were calculated at the MP2/6-31(d) level for calculation of their rotational constants. The calculated rotational constants for CH_3SCH_3 (A, B, C) and $CH_3SCH_3^+$ (A^+, B^+, C^+) are listed in Table 1. At the MP2/6-31G(d) level of theory, the geometries for both CH_3SCH_3 and $CH_3SCH_3^+$ are predicted to have the C_{2v} symmetry. The structural parameters [equilibrium bond distances (r), bond angles (∠), and dihedral angles (φ)] for CH_3SCH_3 and $CH_3SCH_3^+$ are summarized in Table 1. The H^α and H^β represent hydrogen atoms lying in and out of the C–S–C plane, respectively, in CH_3SCH_3 and $CH_3SCH_3^+$. The differences in the theoretical bond lengths [r(C–S), r(C–H^α), and r(C–H^β)], bond angles [∠C–S–C, ∠S–C–H^α, and ∠S–C–H^β], and dihedral angles [φ(C–S–C–H^α) and φ(C–S–C–H^β)] for CH_3SCH_3 and $CH_3SCH_3^+$ are also calculated in Table 1.

3. Results and discussion

3.1. Photoionization efficiency spectrum for CH_3SCH_3

The adiabatic IE of CH_3SCH_3 has been measured to be 8.685 ± 0.005 eV (70049 ± 40 cm^{-1})[27] by Watanabe et al. and 8.69 ± 0.01 eV (70090 ± 81 cm^{-1}) [28] by Akopyan et al. in previous PIE studies. The G2 calculation of the present study gives an IE(CH_3SCH_3) value of 8.71 eV (70251 cm^{-1}), and is in good agreement with these PIE measurements. Similar to the N2P ionization study of CH_3CH_2SH, efforts to measure the N2P-PIE spectrum for CH_3SCH_3 were not successful. As pointed out previously [20,21], the N2P ionization requires the laser to be focused at the PEX/PI region. Thus, parent $CH_3SCH_3^+$ ions initially formed by the N2P ionization may absorb an additional photon within the same laser pulse, and result in further dissociation. The VUV-PIE spectrum for CH_3SCH_3 obtained using a dc electric fields (F) of 42 V/cm at the PEX/PI region is

Table 1
Calculated rotational constants (A″/A^+, B″/B^+, and C″/C^+), bond lengths (r), bond angles (∠), and dihedral angles (φ) for CH_3SCH_3/$CH_3SCH_3^+$ obtained at the MP2/6-31G(d) level of theory

	CH_3SCH_3	$CH_3SCH_3^+$	Δ (ion − neutral)[a]
Rotational constants[b] (cm^{-1})			
A″ or A^+ (cm^{-1})	0.589	0.639	—
B″ or B^+ (cm^{-1})	0.256	0.249	—
C″ or C^+ (cm^{-1})	0.191	0.192	—
Bond lengths[c] (Å)			
r(C–S)	1.804	1.784	−0.020
r(C–H^α)	1.091	1.090	−0.001
r(C–H^β)	1.092	1.095	+0.003
Bond angles[c] (deg.)			
∠C–S–C	98.5	102.5	+4.0
∠S–C–H^α	107.7	108.2	+0.5
∠S–C–H^β	111.3	109.3	−2.0
Dihedral angles[c] (deg.)			
φ(C–S–C–H^α)	180.0	180.0	0.0
φ(C–S–C–H^β)	61.1	59.8	−1.3

[a] Difference of the bond parameter predicted for $CH_3SCH_3^+$ and CH_3SCH_3.
[b] The b axis is the C_2 symmetry axis bisecting ∠C–S–C; the a axis is perpendicular to the b axis and lies in the C–S–C plane; and the c axis is perpendicular to the C–S–C plane.
[c] Both CH_3SCH_3 and $CH_3SCH_3^+$ belong to the C_{2v} point group. Here H^α and H^β are hydrogen atoms lying on and out of the C–S–C plane, respectively.

shown in Fig. 1(a). The VUV-PIE spectrum obtained using a higher dc electric field of F = 167 V/cm is depicted in Fig. 1(b). The sharp ionization onsets observed in the PIE spectra indicate that the Franck–Condon factor for the ionization transition is favorable. Since the ionization of CH_3SCH_3 involves the removal of a nonbonding electron localized at the S atom, the geometries for CH_3SCH_3 and $CH_3SCH_3^+$ are expected to be similar. Assuming that the IE is determined by the midpoint of the rapidly rising ionization onset in the PIE spectrum, we obtained IE(CH_3SCH_3) values of 70 032 ± 12 cm^{-1} and 70 060 ± 12 cm^{-1} for F = 167 and 42 V/cm, respectively. The lower IE value observed for F = 167 V/cm than that for F = 42 V/cm is due to the Stark shift effect. By linear extrapolation, the IE at zero electric field is determined to be 70 088 ± 12 cm^{-1}.

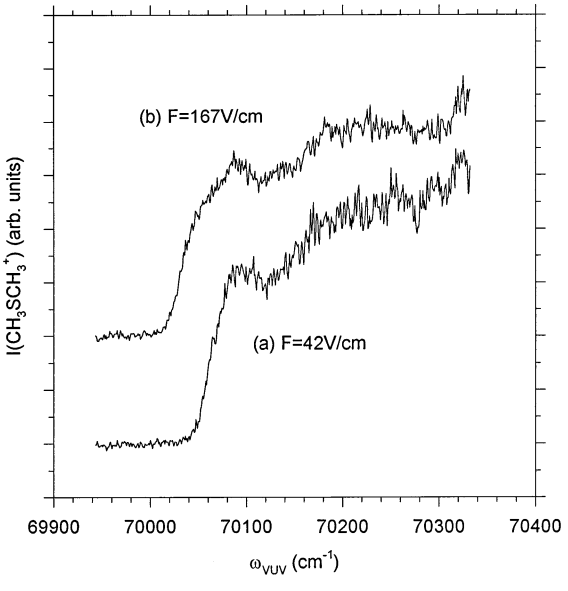

Fig. 1. VUV-PIE spectrum of CH_3SCH_3 in the photon energy range of 69 940–70 330 cm^{-1} recorded using a dc electric field of (a) 42 V/cm and (b) 167 V/cm.

3.2. Comparison and assignment of the VUV-PFI-PE and N2P-PFI-PE spectra for CH_3SCH_3

In both the VUV and N2P experiments, we have measured the PFI-PE spectrum of CH_3SCH_3 covering the energy region of 69 500–72 500 cm^{-1}. The

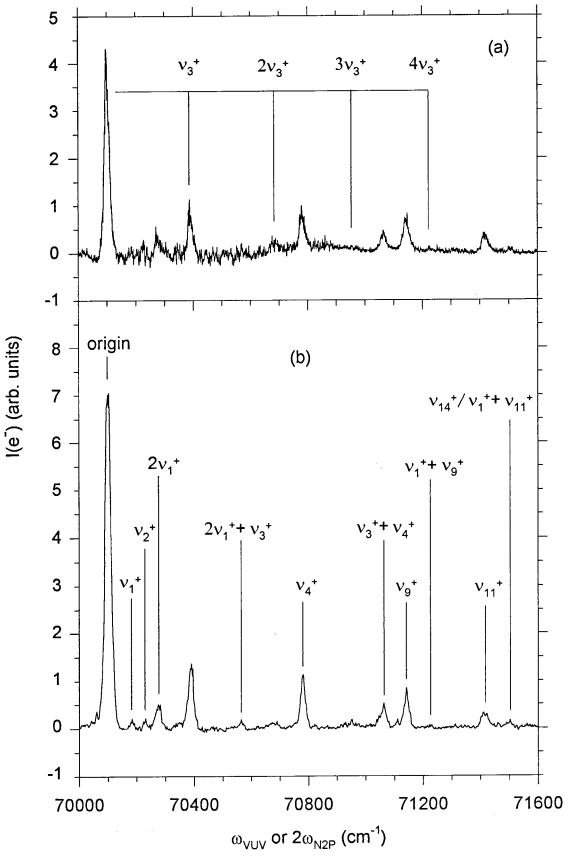

Fig. 2. VUV-PFI-PE spectrum (a) and N2P-PFI-PE spectrum (b) of CH_3SCH_3 in the photon energy range of 70 000–71 600 cm^{-1}. The observed ν_3^+ (symmetric C–S–C bending) vibrational progression for $CH_3SCH_3^+$ is marked in (a). Other assignments of $CH_3SCH_3^+$ vibrational bands are marked in (b). See also Table 2 for the assignments.

VUV-PFI-PE and N2P-PFI-PE spectra in the energy region of 70 000–71 600 cm^{-1} are plotted in Fig. 2(a) and (b), respectively. The spectra of Fig. 2(a) and (b) represent the average of more than two independent scans. The signal-to-noise ratio obtained for the N2P-PFI-PE spectrum is better than that for the VUV-PFI-PE spectrum. Taking into account the experimental uncertainties, we conclude that the vibrational bands and their relative intensities observed in the two spectra are nearly identical. The major peaks at 70 094 cm^{-1} observed in Fig. 2(a) and (b) have FWHMs of ≈20 cm^{-1} and are assigned as the origin band, corresponding to the ionization transition CH_3SCH_3 ($\tilde{X}\ ^1A_1$; $v_i = 0$) → $CH_3SCH_3^+$ ($\tilde{X}\ ^2B_1$; $v_i^+ = 0$) + e^-. The overwhelmingly high intensity for the origin band is consistent with the prominent ionizing steplike onset observed in the PIE spectrum of Fig. 1. The widths of the vibrational PFI-PE bands resolved in Fig. 2(a) and (b) can be attributed to finite rotational excitation of the CH_3SCH_3 sample. As shown in the spectral simulation below (Sec. 3.3), the rotational temperature for CH_3SCH_3 achieved in the pulsed supersonic expansion is ≈30 K.

In our recent PFI-PE study of CH_3CH_2SH [20], we suggested that the comparison of corresponding theoretical structural parameters, such as bond lengths, bond angles, and dihedral angles, for the neutral and cation is useful in revealing the excitation vibrational modes of the cation. As shown in Table 1, the change in r(C–S) is significantly greater than those for r(C–H$^\alpha$) and r(C–H$^\beta$) upon ionization of CH_3SCH_3. This observation indicates that the C–S stretching mode is excited in $CH_3SCH_3^+$. Similarly, since finite changes are predicted for ∠C–S–C, ∠S–C–H$^\beta$, and φ(C–S–C–H$^\beta$) upon ionization of CH_3SCH_3, we expect that the C–S–C bending, S–C–H$^\beta$ bending, and torsional modes in $CH_3SCH_3^+$ are also excited. Assuming that the CH_3SCH_3 sample is vibrationally cold, the total vibrational wave function for CH_3SCH_3 in its ground electronic state should be totally symmetric and have the a_1 symmetry. In accordance with the Franck–Condon principle, which results from the Born–Oppenheimer approximation, the allowed ionization transitions should give rise to $CH_3SCH_3^+$ vibrational states with a_1 symmetry. Guided by the ab initio harmonic frequencies and their symmetries, we have satisfactorily assigned the vibrational bands resolved in the VUV-PFI-PE and N2P-PFI-PE spectra. The comparison between the experimental and theoretical harmonic vibrational frequencies is given in Table 2. Here, the energies of the observed vibrational PFI-PE bands are measured with respect to the peak position of the origin band. The assignments of the vibrational bands are also marked in Fig. 2(a) and (b).

According to theoretical predictions, the two lowest harmonic frequencies for $CH_3SCH_3^+$ are the asymmetric torsional mode (ν_1^+, predicted frequency = 57 cm^{-1}) and symmetric torsional mode (ν_2^+, predicted

Table 2
Comparison of experimental and theoretical vibrational frequencies for $CH_3SCH_3^+$

Assignment[a]	N2P-PFI-PE (cm^{-1})[b,c]	VUV-PFI-PE (cm^{-1})[b,c]	Theoretical[d,e] (cm^{-1})
ν_1^+	83 (w)	86 (w)	57 [asym. torsional (a_2)]
ν_2^+	130 (w)	130 (w)	134 [sym. torsional (b_1)]
$2\nu_1^+$	175 (s)	173 (s)	114
	(166)	(172)	
ν_3^+	291 (s)	290 (s)	276 [C–S–C bending (a_1)]
$2\nu_1^+ + \nu_3^+$	465 (w)	472 (w)	410
	(466)	(463)	
$2\nu_3^+$	577 (w)	578 (w)	$2\nu_3^+ = 552$
	(582)	(580)	
ν_4^+	681 (s)	681 (s)	675 [sym C–S stretch (a_1)]
$3\nu_3^+$	865 (w)	865 (w)	$3\nu_3^+ = 828$
	(873)	(870)	
$\nu_3^+ + \nu_4^+$	963 (s)	967 (s)	951
	(972)	(971)	
ν_9^+	1042 (s)	1042 (s)	1057 [S–C–H bending (a_1)]
$\nu_1^+ + \nu_9^+$	1131 (w)	1127 (w)	1114
	(1128)	(1125)	
$4\nu_3^+$	(1164)	(1160)	$4\nu_3^+ = 1104$
ν_{11}^+	1312 (s)	1316 (s)	1356 [S–C–H bending + wagging (a_1)]
ν_{14}^+	1402 (w)	1409 (w)	1416 [S–C–H bending + scissoring + wagging (a_1)]
$\nu_1^+ + \nu_{11}^+$	(1395)	(1402)	1413

[a] See the text. The frequencies for ν_n^+ are arranged in increasing order as a function of n.
[b] We denote (s) and (w) as strong and weak intensities, respectively.
[c] The frequencies given in parentheses are estimated energy positions based on experimental observations. For $2\nu_2^+$ and $n\ \nu_3^+$, the estimated values have not taken into account corrections due to anharmonicities.
[d] Calculated frequencies at the MP2/6-31G(d) level of theory. The theoretical values have been scaled by 0.92.
[e] The σ-plane perpendicular to the C–S–C plane is taken as the σ_v in the symmetry labels.

frequency = 134 cm^{-1}). The three lowest energy bands observed in the VUV-PFI-PE/N2P-PFI-PE spectra are peaked at 83/86, 130/130, and 175/173 cm^{-1}. If we assign the first peak at 83/86 cm^{-1} to ν_1^+, the third peak at 175/173 cm^{-1} should be assigned to $2\nu_1^+$. The second peak at 130/130 cm^{-1} can be assigned to ν_2^+. Since $2\nu_1^+$ has a_1 symmetry, this assignment accounts for the higher intensity observed for the peak at 175/173 cm^{-1} compared to those of the first and second peaks. We expect that the torsional potentials for CH_3SCH_3 and $CH_3SCH_3^+$ are highly anharmonic. As shown in the VUV-PFI-PE/N2P-PFI-PE study of CH_3CH_2SH [20], more accurate predictions for ionization transitions associated with the $CH_3SCH_3/CH_3SCH_3^+$ torsional modes will require the consideration of transitions between energy levels supported by the torsional potential for CH_3SCH_3 and those for $CH_3SCH_3^+$.

All other vibrational bands observed at higher energies can be assigned to $CH_3SCH_3^+$ vibrational modes with a_1 symmetry. The three strong vibrational bands observed in the VUV-PFI-PE/N2P-PFI-PE spectra at 290/291, 681/681, and 1042/1042 cm^{-1} can be assigned with confidence to the ν_3^+ (symmetric C–S–C bending mode), ν_4^+ (symmetric C–S stretching mode), and ν_9^+ (symmetric S–C–H bending mode) for $CH_3SCH_3^+$. These modes are of a_1 symmetry and have the respective scaled MP2/6-31G(d) harmonic frequencies of 276, 675, and 1057 cm^{-1}. The weak structures at 578/577, 865/865, and 1127/1131 cm^{-1} are assigned as $2\nu_3^+$, $3\nu_3^+$, and $4\nu_3^+$, respectively, belonging to members of the ν_3^+ vibrational progression. The weak band at 1127/1131 cm^{-1} may also arise from excitation of $\nu_1^+ + \nu_9^+$. The medium peaks observed at 472/465, 967/963, and 1316/1312 cm^{-1} are assigned to $2\nu_1^+ + \nu_3^+$, $\nu_3^+ + \nu_4^+$ and ν_{11}^+

(symmetric S–C–H bending and wagging mode) of $CH_3SCH_3^+$, respectively. Based on the observed energies for ν_1^+, ν_3^+ and ν_4^+, the $2\nu_1^+ + \nu_3^+$ and $\nu_3^+ + \nu_4^+$ combination bands are expected to be at 463–466 and 971–972 cm^{-1}, respectively. The weak peak at 1409/1402 cm^{-1} can be attributed to ν_{14}^+ (symmetric S–C–H bending + scissoring + wagging, predicted frequency = 1416 cm^{-1}) and/or $\nu_1^+ + \nu_{11}^+$. The latter combination band is expected to appear at 1399/1398 cm^{-1}. Both the ν_{11}^+ and ν_{14}^+ are of a_1 symmetry. Comparing the theoretical and experimental vibrational frequencies, we conclude that the scaled MP2/6-31G(d) frequencies are too low for ν_n^+ ($n \leq 4$) and too high for ν_n^+ (n = 9, 11, and 14).

3.3. Simulation of the origin VUV-PFI-PE band for $CH_3SCH_3^+$

Fig. 3(a) shows an expanded view of the origin band of the VUV-PFI-PE spectrum for CH_3SCH_3 in the energy region of 70 060–70 130 cm^{-1}. This spectrum represents the average of more than five independent scans. The majority of fine structures of Fig. 3(a) are reproducible. The most noticeable feature is the dip in the center of the PFI-PE band. This feature is contrary to the sharp peaks observed in the centers of the VUV-PFI-PE origin bands for CH_3SH and CH_3CH_2SH [21].

Both CH_3SCH_3 and $CH_3SCH_3^+$ are asymmetric top molecules that are classified by the moment of inertia I_A, I_B, and I_C associated with rotation around the a, b, and c molecular axes, respectively [29,30]. For CH_3SCH_3 and $CH_3SCH_3^+$, the symmetry axis z bisecting the ∠C–S–C is identical to the b axis, the molecular a axis (symmetry axis y) is perpendicular to the b axis and lies in the C–S–C molecular plane, and the molecular c axis (symmetry axis x) is perpendicular to the C–S–C molecular plane. The similar theoretical rotational constants obtained for CH_3SCH_3 and $CH_3SCH_3^+$ (see Table 1) are consistent with the fact that the neutral and cationic geometries are quite similar. As indicated above, both CH_3SCH_3 and $CH_3SCH_3^+$ belong to the C_{2v} point group. The asymmetry parameters (κ) [defined as (2B″–A″–C″)/(A″–C″) for the neutral and $2B^+–A^+–C^+/A^+–C^+$) for the

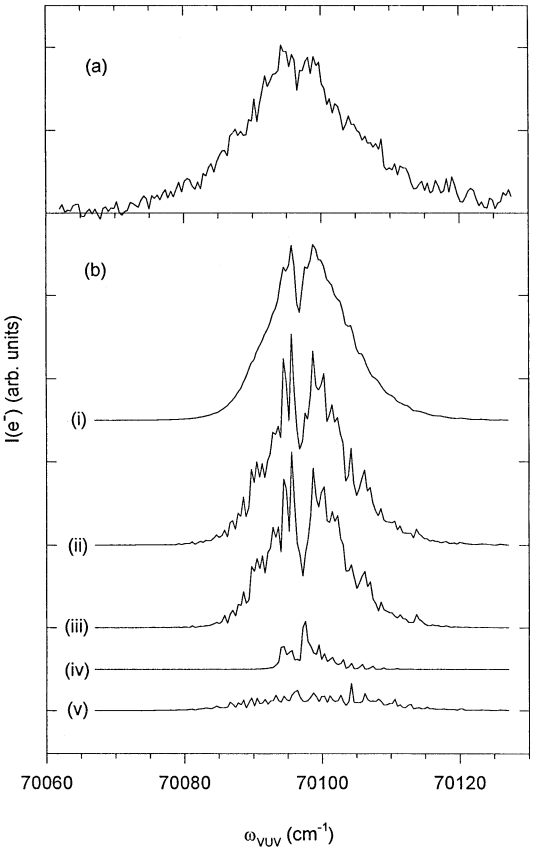

Fig. 3. (a) The origin VUV-PFI-PE band for $CH_3SCH_3^+$ in the energy range of 70 060–70 160 cm^{-1}. (b) Simulated spectra for CH_3SCH_3 obtained by using a rotational temperature of 30 K and a Gaussian width of 0.8 and 0.2 cm^{-1} (FWHM) are marked as curves (i) and (ii), respectively. The respective contributions by the Q branches ($\Delta J = 0$, $\Delta K = 0, \pm 1$) and P plus R branches ($\Delta J = \pm 1$, $\Delta K = 0, \pm 1$) calculated assuming a Gaussian linewidth of 0.2 cm^{-1} (FWHM) are shown as curves (iv) and (iii). The calculated contribution [Gaussian linewidth = 0.2 cm^{-1} (FWHM)] due to rotational branches ($\Delta J = 0, \pm 1$; $\Delta K = \pm 2$) is shown as curve (v). The r_B values used for ($\Delta J = \pm 1$, $\Delta K = 0, \pm 1$) are 5, whereas the r_B values for all other rotational branches are taken to be 1.

ion] are −0.67 for CH_3SCH_3 and −0.74 for $CH_3SCH_3^+$. Since these κ values are close to −1, CH_3SCH_3 and $CH_3SCH_3^+$ are near prolate top molecules [29,30].

We have calculated the rotational energies (E_{rot}) of these asymmetric top molecules by diagonalization of the Hamiltonian matrix using the symmetric top rotational basis set [29]. The asymmetric top energy

levels for CH_3SCH_3 and $CH_3SCH_3^+$ are labeled by $J''_{K''_aK''_c}$ and $J^+_{K_a^+K_c^+}$, respectively. Here, J'' and J^+ are good quantum numbers that represent the respective total angular momentum quantum numbers for the neutral and cation. The project quantum numbers K''_a (K_a^+) and K''_c (K_c^+) are good quantum numbers only in the prolate and oblate top limits, respectively. Here, we use the conventional labeling *O*, *P*, *Q*, and *R* and *S* rotational branches for $\Delta J = N^+ - J'' = -2, -1, 0, +1$, and $+2$ transitions, respectively.

Depending on the order of the rotational constants and the direction of the transition dipole moment, rotational transitions involving asymmetric top molecules are classified into types a, b, and c transitions. The $CH_3SCH_3/CH_3SCH_3^+$ system of interest here is similar to that of the H_2O/H_2O^+ that has been investigated in detail [31]. The highest occupied orbital for H_2O (CH_3SCH_3) has the b_1 symmetry and is essentially a *p*-type atomic orbital pointing out the H–O–H (C–S–C) molecular plane. Thus, the atomic selection rules $\Delta l = \pm 1$ are expected to provide an approximated description of photoionization for these molecules. Ab initio Schwinger variational calculations on the H_2O/H_2O^+ system indicate dominant kd ($l = 2$) photoionization continuum, in accordance with the atomic model [32]. Calculations based on the multichannel quantum defect theory (MQDT) show that $l = 2$ photoionization leads only to type c rotational transitions, for which the selection rules are ΔK_a = odd; and ΔK_c = even [33]. Rotationally resolved VUV-PFI-PE spectrum for H_2O near its ionization threshold has been reported previously by White and co-workers [34]. Although the strongest transitions can be assigned to type c transitions, rotational structures arising from type a transitions are clearly observed. This observation is attributed to np–nd Rydberg series interactions induced by a finite anisotropy of the H_2O^+ ion core [35,36]. In the MQDT approach, the np–nd mixing could also be induced by a long-range dipolar coupling, which is the manifestation of the anisotropy of the cation potential. The types a and c transitions for the H_2O/H_2O^+ system are a general consequence of the parity selection rule for the formation of an l = even (odd) electron. The ab initio Schwinger variational study of McKoy and co-workers has shown that for threshold photoionization of H_2O the selection rules are summarized as $\Delta K_a + l$ = odd [36,37]. They show that only type c (l = even) and type a (l = odd) photoionization transitions are allowed independent of nuclear symmetry constraints. In view of the similarity between the H_2O/H_2O^+ and $CH_3SCH_3/CH_3SCH_3^+$ systems, we may assume that the threshold photoionization of CH_3SCH_3 also follows types a and c transitions. However, our effort to simulate the VUV-PFI-PE spectrum of Fig. 3(a) by assuming types a and c transitions was unsuccessful. Since individual rotational transitions are not resolved in the present experiment, this unsuccessful simulation cannot be considered as proof that the selection rules governing photoionization transitions for the H_2O/H_2O^+ and $CH_3SCH_3/CH_3SCH_3^+$ systems are different.

As shown in Table 1, the rotational constants A″ and A^+ are significantly greater than C″ and C^+ indicating that the rotational spacings of CH_3SCH_3 and $CH_3SCH_3^+$ are mostly determined by the A″ and A^+ rotational constants, respectively. In the simulation present below, we have assumed that the photoionization transitions for the $CH_3SCH_3/CH_3SCH_3^+$ are close to the prolate top limit [29,30], governed by ΔK_a ($=\Delta K$) only.

The intensity for a rotational transition from a neutral level $|J'', K''_a, K''_c>$ to an ionic state $[I_{PE}(J'', K''_a, K''_c)]$ is proportional to the rotational population of the neutral molecule according to the Boltzmann distribution [21,23],

$$I_{PE}(J'', K''_a, K''_c) \propto r_B(2J'' + 1) \exp[-\Delta E_{rot}/(kT_{rot})] \quad (1)$$

Here, T_{rot} is the rotational temperature of CH_3SCH_3, ΔE_{rot} is the rotational energy measured with respect to the ground rovibronic state of CH_3SCH_3, and r_B is a scaling parameter for a given rotational branch that is adjusted to obtain the best fit to the experimental spectrum. The main assumption of this semiempirical scheme is that the transition probabilities from different $|J'', K''_a, K''_c>$ levels within a rotational branch are

taken to be equal and are measured by the scaling parameter r_B. In an accurate theoretical treatment, the intensity of a rotational transition is proportional to the product of the rotational population and the rotational line strength, which depends on the actual electronic matrix element that couple the initial neutral rotational state to the final cation rotational state, plus the photoelectron state.

Curve (i) of Fig. 3(b) shows the simulated spectrum for CH_3SCH_3 obtained using a T_{rot} value of 30 K and a Gaussian line width of 0.8 cm^{-1} (FWHM). In order to compare the experimental and simulated features, we have also shown the simulated spectrum calculated using a Gaussian line width of 0.2 cm^{-1} (FWHM) [see curve (ii)]. The contributions by the Q branches ($\Delta J = 0$; $\Delta K = 0, \pm 1,$) and the P plus R branches ($\Delta J = \pm 1$; $\Delta K = 0, \pm 1$) calculated assuming a Gaussian line width of 0.2 cm^{-1} (FWHM) are plotted as curves (iv) and (iii) in Fig. 3(b), respectively. The rotational branches ($\Delta J = 0, \pm 1$; $\Delta K = \pm 2$) calculated using a Gaussian line width of 0.2 cm^{-1} (FWHM) are also shown in Fig. 3(b) [see curve (v)]. These $\Delta K = \pm 2$ branches are quite broad. The r_B values used for the rotational branches ($\Delta J = \pm 1$, $\Delta K = 0, \pm 1$) are 5, as compared to the r_B values of 1 for all other rotational branches.

Although the simulated spectrum consisting of the P, Q, and R rotational branches captures the main structures observed in the VUV-PFI-PE spectrum of Fig. 3(a), the width of such a simulated spectrum [curve (i) or (ii)] is too narrow compared to the experimental spectrum. We expect that higher rotational branches, i.e. $|\Delta J| > 1$ branches [not shown in Fig. 3(b)], also have minor contributions to the experimental spectrum. The contributions of the $|\Delta J| > 1$ branches should have the effect of broadening the simulated band and thus providing a more satisfactory fit to the experimental spectrum. The most important goal of the simulation is to obtain an accurate value for the adiabatic IE for CH_3SCH_3. Taking into account the uncertainty of the simulation model, the spectral simulation yields a value of 70 097.3 ± 2.0 cm^{-1} (8.69096 ± 0.00016 eV) for the IE for CH_3SCH_3.

4. Conclusion

We have obtained the vibrationally resolved VUV-PFI-PE and N2P-PFI-PE spectra for CH_3SCH_3 near its ionization threshold. Guided by the theoretical harmonic frequencies for $CH_3SCH_3^+$, we have assigned the photoelectron bands to excitations of the torsional (ν_1^+ and ν_2^+), C–S–C bending (ν_3^+), symmetric C–S stretching (ν_4^+), and S–C–H bending (ν_9^+, ν_{11}^+, ν_{14}^+) vibrational modes of $CH_3SCH_3^+$.

Contours of rotational branches are partially resolved in the origin band of the VUV-PFI-PE spectrum. Using the theoretical rotational constants based on the geometries for CH_3SCH_3 and $CH_3SCH_3^+$ predicted at the MP2/6-31G(d) level, we have calculated the rotational levels of these asymmetric top molecules. On the basis of a semiempirical simulation, we have obtained an accurate value for the adiabatic IE of CH_3SCH_3.

Acknowledgements

The authors thank Dr. C.-W. Hsu and Dr. J.-C. Huang for their assistance in the early phase of this experiment. This work was supported by the Director, Office of Energy Research, Office of Basic Energy Sciences, Chemical Science Division of the U.S. Department of Energy under Contract No. W-7405-Eng-82 for the Ames Laboratory. Y.-S.C. was the recipient of the Henry Gilman Fellowship and the Nelson Chemistry Scholarship for 1996–1997. Ames Laboratory is operated for the U.S. Department of Energy by Iowa State University under Contract No. W-7405-Eng-82.

References

[1] S.G. Lias, J.E. Bartmess, J.F. Liebman, L. Holmes, R.D. Levin, W.G. Mallard, J. Phys. Chem. Ref. Data 17 (1988) (Suppl).
[2] H.M. Rosenstock, M.K. Draxl, B.W. Steiner, J.T. Herron, J. Phys. Ref. Data 6 (1977) (Suppl.).
[3] D.W. Turner, C. Baker, A.D. Baker, C.R. Brundle, Molecular Photoelectron Spectroscopy, Wiley, London, 1970.
[4] K. Kimura, S. Katsumata, Y. Achibi, T. Yamazaki, S. Iwata,

Handbook of He I Photoelectron Spectra of Fundamental Organic Molecules, Halsted Press, 1981.
[5] W.-K. Li, S.-W. Chiu, Z.-X. Ma, C.-L. Liao, C.Y. Ng, J. Chem. Phys. 99 (1993) 8440.
[6] K. Raghavachar, B.B. Stefanov, L.A. Curtiss, J. Chem. Phys. 106 (1997) 6764; and references therein.
[7] C.Y. Ng, in T. Baer, C.Y. Ng, I. Powis (Eds.), The Structure, Energetics, and Dynamics of Organic Ions, Wiley Series in Ion Chem. and Phys., Wiley, Chichester, 1996, pp. 35–124; C.Y. Ng, in Volman, Hammond, Neckers (Eds.), Adv. Photochemistry, Wiley, New York, 1997, Vol. 22, p. 1.
[8] D.P. Chong, C.Y. Ng, J. Chem. Phys. 98 (1993) 759.
[9] J.W. Hepburn, in C.Y. Ng (Ed.), Vacuum Ultraviolet Photoionization and Photodissociation of Molecules and Clusters, World Scientific, Singapore, 1991, p. 435.
[10] J.W. Hepburn, in A. Meyers, T.R. Rizzo (Eds.), Laser Techniques in Chemistry, Wiley, New York, 1994.
[11] A.H. Kung, Y.T. Lee, in C.Y. Ng (Ed.), Vacuum Ultraviolet Photoionization and Photodissociation of Molecules and Clusters, World Scientific, Singapore, 1991, p. 487.
[12] I. Powis, T. Baer, C.Y. Ng (Eds.), High Resolution Laser Photoionization and Photoelectron Studies, Wiley Series in Ion Chemistry and Physics, Wiley, Chichester, 1995; and references therein.
[13] K. Müller-Dethlefs, M. Sander, E.W. Schlag, Z. Naturforsch. A 39a (1984) 1089.
[14] K. Müller-Dethlefs, E.W. Schlag, Ann. Rev. Phys. Chem. 42 (1991) 109.
[15] A. Strobel, I. Fischer, J. Staecker, G. Niedner-Schatteburg, K. Müller-Dethlefs, V.E. Bondybey, J. Chem. Phys. 97 (1992) 2332.
[16] I. Fischer, A. Lochschmidt, A. Strobel, G. Niedner-Schatteburg, K. Müller-Dethefs, V.E. Bondybey, Chem. Phys. Lett. 202 (1993) 542.
[17] C.-W. Hsu, M. Evans, C.Y. Ng, P. Heimann, Rev. Sci. Instrum. 68 (1997) 1694.
[18] C.-W. Hsu, M. Evans, S. Stimson, C.Y. Ng, P. Heimann, J. Chem. Phys. 106 (1997) 8931.
[19] An up-to-date reference list for PFI-PE studies of molecules and radicals can be found at the ZEKE Website (http://eos.phys.chemie.tu-muenchen.de/zeke).
[20] Y.-S. Cheung, C.-W. Hsu, C.Y. Ng, W.-K. Li, S.-W. Chiu, Int. J. Mass Spectrom. Ion Processes 159 (1996) 13.
[21] Y.-S. Cheung, J.-C. Huang, C.Y. Ng, J. Chem. Phys. 109 (1998) xxxx
[22] M.J. Frisch et al., GAUSSIAN 94, Gaussian, Pittsburgh, PA, 1994.
[23] C.-W. Hsu, C.Y. Ng, J. Chem. Phys. 101 (1994) 5596.
[24] C.-W. Hsu, D.P. Baldwin, C.-L. Liao, C.Y. Ng, J. Chem. Phys. 100 (1994) 8047.
[25] J.-C. Huang, Y.-S. Cheung, M. Evans, C.-X. Liao, C.Y. Ng, C.-W. Hsu, P. Heimann, H. Lefebvre-Brion, C. Cossart-Magos, J. Chem. Phys. 106 (1997) 864.
[26] S.-W. Chiu, W.-K. Li, W.-B. Tzeng, C.Y. Ng, J. Chem. Phys. 97 (1992) 6557.
[27] K. Watanabe, T. Nakayma, J. Mottl, J. Quant. Spectrosc. Radiat. Trans. 2 (1962) 369.
[28] M.E. Akopyon, Y.L. Sergeev, F.I. Vilesov, Khim. Vys. Energ. 4 (1970) 305 [English translation, High Energy Chem. 4 (1970) 265].
[29] P.F. Bernath, Spectra of Atoms and Molecules, Oxford Univ. Press, Oxford, 1995.
[30] G. Herzberg, Molecular Spectra and Molecular Structure III. Electronic Spectra and Electronic Structure of Polyatomic Molecules, Van Nostrand, New York, 1966.
[31] R.T. Wiedmann, M.G. White, in I. Prowis, T. Baer, C.Y. Ng (Eds.), High Resolution Laser Photoionization and Photoelectron Studies, Wiley Series in Ion Chem. and Phys., Wiley, Chichester, 1995, p. 79; and references therein.
[32] L.E. Machdo, L.M. Brescansin, M.A.P. Lima, M. Braunstein, V. McKoy, J. Chem. Phys. 92 (1990) 2362.
[33] M.S. Child, Ch. Jungen, J. Chem. Phys. 93 (1990) 7756.
[34] R.G. Tonkyn, R.T. Wiedmann, E.R. Grant, M.G. White, J. Chem. Phys. 95 (1991) 7033.
[35] R.D. Gilbert, M.S. Child, Chem. Phys. Lett. 187 (1991) 153.
[36] M.-T. Lee, K. Wang, V. McKoy, R.G. Tonkyn, R.T. Wiedmann, E.R. Grant, M.G. White, J. Chem. Phys. 96 (1992) 7848.
[37] M.-T. Lee, K. Wang, V. McKoy, J. Chem. Phys. 97 (1992) 3108.